

---

---

## LONG-TERM VARIATIONS IN PEAK ELECTRON DENSITY AND TEMPERATURE OF MESOPAUSE REGION: DEPENDENCE ON SOLAR, GEOMAGNETIC, AND ATMOSPHERIC ACTIVITIES, LONG-TERM TRENDS

---


---

G.A. Zharebtsov 

Institute of Solar-Terrestrial Physics SB RAS,  
Irkutsk, Russia, gaz@iszf.irk.ru

K.G. Ratovsky 

Institute of Solar-Terrestrial Physics SB RAS,  
Irkutsk, Russia, ratovsky@iszf.irk.ru

I.V. Medvedeva 

Institute of Solar-Terrestrial Physics SB RAS,  
Irkutsk, Russia, ivmed@iszf.irk.ru

---

**Abstract.** The paper overviews the main results of the study of long-term variations in characteristics of the upper neutral atmosphere and ionosphere, obtained during the implementation of Russian Science Foundation Project No. 22-17-00146 “Experimental and theoretical study of the coupling neutral and ionized components of Earth’s atmosphere”. We study and compare long-term variations in the peak electron density and temperature of the mesopause region. Their dependences on solar, geomagnetic, and atmospheric activity, as well as long-term trends, are analyzed. The analysis is based on data from long-term measurements with the ISTP SB RAS complex of instruments. The peak electron density ( $N_mF2$ ) data was acquired with the Irkutsk analog automatic ionospheric station for 1955–1996 and the Irkutsk digital ionosonde DPS-4 for 2003–2021. The atmospheric temperatures at mesopause altitudes ( $T_m$ ) were obtained from spectrometric observations of the hydroxyl molecule emission (OH (6-2) band, 834.0 nm, emission maximum height ~87 km) for 2008–2020. The

analysis uses solar ( $F10.7$ ) and geomagnetic ( $A_p$ ) activity indices, as well as data on variations in the Southern Oscillation Index (SOI). The study employs simple and multiple linear regression methods. Annual average  $N_mF2$  values are found to be predominantly controlled by changes in solar flux. Analysis of regression residuals shows that the largest deviations from regression (for both simple and multiple regression) are observed in years near the maxima of solar cycles 19 (1956–1959) and 22 (1989–1991). Annual average temperature variability in the mesopause region correlates with changes in the SOI index: day-to-day variability exhibits a positive correlation with SOI; and intra-diurnal variability, a negative correlation with SOI. No significant relationship was found between year-to-year variations in the  $N_mF2$  and  $T_m$  variability.

**Keywords:** long-term variations, peak electron density, temperature, mesopause region, solar activity, geomagnetic activity, long-term trends

---

### INTRODUCTION

Studying long-term variations in characteristics of the upper atmosphere is extremely relevant and important for understanding climate changes at these altitudes. It is well known that long-term (one to several solar cycles) variations in ionospheric parameters, averaged by month, season or year, are generally due to variations in solar activity [Laštovička, 2019; Danilov, Konstantinova, 2020; Bremer, 1998]. Variations in geomagnetic activity can make an additional contribution. Along with variations associated with solar and geomagnetic activity, there may be long-term trends reflecting climatic changes over several solar cycles. Variability in ionospheric parameters depends on geomagnetic and solar activity, as well as dynamic processes in the lower atmosphere [Forbes et al., 2000; Rishbeth, Mendillo, 2001; Araujo-Pradere et al., 2005; Deminov et al., 2013]. It has been found in [Rishbeth and Mendillo, 2001; Forbes et al., 2000] that the contribution of geomagnetic activity to ionospheric disturbances is comparable to the effect of the lower atmosphere and much more significant than disturbances caused by short-term variations in solar activity.

The temperature regime of the mesopause region (80–100 km) is actively affected by both solar radiation and energy dissipation of wave processes occurring in the lower atmosphere. Atmospheric temperature variability at these altitudes indicates many climatic and meteorological processes in the lower and middle atmosphere. Seasonal variations in the mesopause temperature  $T_m$ , maximum in winter and minimum in summer, are the most pronounced; temperature differences can be as large as 60 K. Day-to-day and intradiurnal temperature variability is mainly driven by wave processes — migrating planetary waves, tides, and internal gravity waves (IGWs). The  $T_m$  variability caused by atmospheric waves of different time scales also depends strongly on season and can differ significantly according to the region of observation [Offermann et al., 2009; Perminov et al., 2014a, b]. Of particular interest are year-to-year variations and long-term trends in  $T_m$ . They are driven by the combined effect of long-term variations in solar activity and climatic changes in the lower and middle atmosphere [Khomich et al., 2008; Beig, 2011]. Quasi-two-year oscillations, the effect of solar activity, and a long-term trend have been found in year-to-year  $T_m$  variations [Semenov, 2008; Khomich et al., 2008; Beig, 2011].

This paper overviews the main results of the study of long-term variations in characteristics of the upper neutral atmosphere and the ionosphere, obtained during the implementation of RSF Project No. 22-17-00146 “Experimental and theoretical study of the coupling neutral and ionized components of Earth’s atmosphere”. We examine and compare long-term variations in the peak electron density  $N_mF2$  and in the temperature of the mesopause region  $T_m$ . Their dependences on solar, geomagnetic and atmospheric activity, as well as long-term trends, are analyzed. The analysis is based on data from long-term measurements with the ISTP SB RAS complex of instruments. Data on  $N_mF2$  for 1955–1996 was obtained at the Irkutsk analog automatic ionospheric station; for 2003–2021, with the Irkutsk digital ionosonde DPS-4;  $T_m$  data, from spectrometric observations of the hydroxyl molecule emission (OH band (6-2), 834.0 nm, emission maximum height ~87 km) in 2008–2020.

The paper is sequel to previous studies that have simultaneously analyzed seasonal variations in  $N_mF2$  and  $T_m$  [Medvedeva, Ratovsky, 2015, 2017]. Their common features and differences have been identified. Year-to-year variations in the parameters considered have been preliminarily analyzed for 2008–2015 in [Medvedeva, Ratovsky, 2017].

## 1. LONG-TERM VARIATIONS IN $N_mF2$ ACCORDING TO VERTICAL SOUNDING DATA FOR 1955–2021

We have examined long-term variations in  $N_mF2$  in the ionosphere over Irkutsk (52° N, 104° E) for 1955–2021. Linear regressions of annual average  $N_mF2$  (separately for nighttime and daytime) on annual average solar and geomagnetic activity indices are used to analyze solar and geomagnetic activity dependences. To analyze long-term trends, we approximate deviations from regressions by a linear time trend.

### 1.1. Data analysis method

To study long-term variations in ionospheric parameters, we have used ionospheric data obtained with Irkutsk ionosondes in 1955–2021, as well as data on the solar and magnetic activity indices  $F10.7$  and  $A_p$  for 1955–2021 [<https://omniweb.gsfc.nasa.gov/form/dx1.html>]. The period considered spans six solar cycles (19–24). As the ionospheric characteristic we take  $N_mF2$  calculated from the critical frequency  $f_oF2$ , determined from ionograms of the ionospheric station AIS or the ionosonde DPS-4 ( $N_mF2 [10^5 \text{ cm}^{-3}] = 0.124 (f_oF2 [\text{MHz}])^2$ ). We analyze annual average  $N_mF2$  for daytime (10–14 LT) and nighttime (22–02 LT), as well as annual average  $F10.7$  and  $A_p$ .

The selected solar and geomagnetic activity indices have been measured for a long time ( $F10.7$  — since 1947,  $A_p$  — since 1932). They are widely used in operational and climatic models of the ionosphere and atmosphere (for example, the global dynamic model of critical frequency of the ionospheric F2 layer [Shubin, Deminov, 2019]; the International Reference Ionosphere (IRI) [Bilitza et al., 2017]; the NRLMSISE-00 empirical

model of the atmosphere [Picone et al., 2002]; the empirical model of the horizontal neutral wind in the upper thermosphere [Drob et al., 2015]). The question as to whether the use of alternative solar and geomagnetic activity indices can give other results requires further research.

To analyze the dependence of  $N_mF2$  on solar activity, we employ a simple linear regression of  $N_mF2$  on  $F10.7$ :  $N_mF2 = N_0 + N_1(F10.7 - 69)$ . The contribution of geomagnetic activity is analyzed using the multiple linear regression of  $N_mF2$  on  $F10.7$  and  $A_p$ :  $N_mF2 = N_0 + N_1(F10.7 - 69) + N_2(A_p - 4)$ . Here  $N_0$  is  $N_mF2$  at solar minimum ( $F10.7 = 69$  s.f.u.  $A_p = 4$ );  $N_1$ ,  $N_2$  are the rates of change in  $N_mF2$  with increasing  $F10.7$  and  $A_p$  respectively.

The first method of estimating the  $N_mF2$  trend involves approximating deviations  $\Delta N_mF2$  from the multiple regression of  $N_mF2$  on  $F10.7$  and  $A_p$  by the linear time trend:  $\Delta N_mF2 = \Delta N_0 + \Delta N_1(\text{year} - 1955)$ ,  $\Delta N_0$  is  $\Delta N_mF2$  in 1955;  $\Delta N_1$  is the trend rate of  $\Delta N_mF2$ . The second method of estimating the  $N_mF2$  trend is based on the analysis of cycle-to-cycle variation in the coefficients of simple regression of  $N_mF2$  on  $F10.7$ .

### 1.2. Results of the analysis of long-term variations in annual average $N_mF2$

The simple linear regression of  $N_mF2$  on  $F10.7$  has demonstrated very high coefficients of determination (98.36 % during the day and 97.13 % at night), with the largest regression errors (negative deviations) observed in 1957–1958 (maximum of solar cycle 19) and 1989–1991 (maximum of cycle 22). A potential source of the errors in simple linear regressions on  $F10.7$  might have been the effect of geomagnetic activity. To test this version, we employed a multiple regression of annual average  $N_mF2$  on annual average  $F10.7$  and  $A_p$ . The results show that geomagnetic activity has virtually no effect on errors in simple linear regressions. The coefficients of determinations of the multiple regressions on  $F10.7$  and  $A_p$  were 98.41 % for daytime and 97.20 % for nighttime, i.e. they coincided with the coefficients of determinations of simple regressions up to 0.1 %.

To identify the causes of errors in the simple linear regression of  $N_mF2$  on  $F10.7$ , we analyzed the scatter diagram of  $N_mF2$  as function of  $F10.7$  (Figure 1). Deviations from the regressions at large values of annual average  $F10.7$  are pronounced. To eliminate the effect of years with high solar activity, we plotted simple regressions of  $N_mF2$  on  $F10.7$  (Figure 2), excluding years for which annual average  $F10.7$  exceeded 175 s.f.u.

When comparing the results of the two regressions, the following can be highlighted. When excluding years with  $F10.7 > 175$  s.f.u., the rate of increase in  $N_mF2$  rises with  $F10.7$ , and  $N_mF2$  decreases at solar minimum. A change in the regression coefficients causes negative deviations from the regression to increase, positive deviations to decrease, with daytime values near the maximum of cycle 21 (1979–1981) fitting well into the new regression curve despite the fact that these values were not considered in the regression with  $F10.7 < 175$  s.f.u.

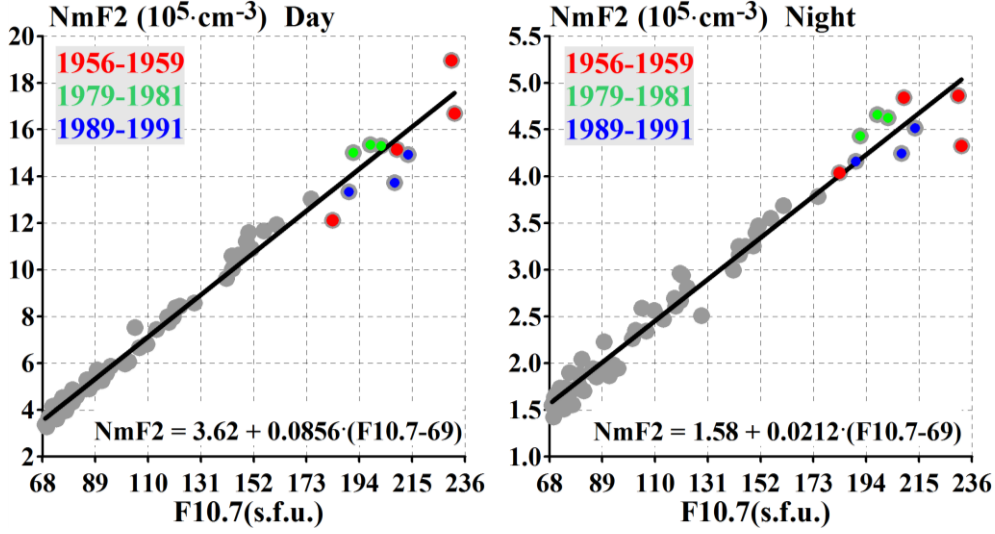


Figure 1. Scatter diagram of annual average  $N_mF2$  as function of annual average  $F10.7$  for daytime (a) and nighttime (b). Values near maxima of solar cycles 19 (1956–1959), 21 (1979–1981), and 22 (1989–1991) are shown in red, green, and blue respectively

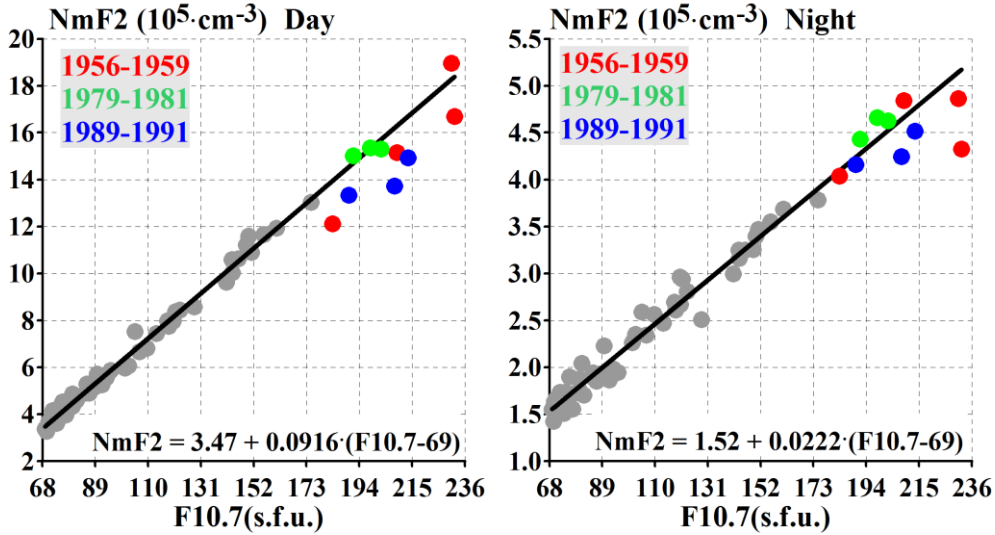


Figure 2. The same as in Figure 1 except for the years with  $F10.7 > 175$  s.f.u.

This fact suggests that the cause of regression errors is not linked to high solar activity per se. The deviation from the regression curves in the years near the maximum of solar cycle 22 (1989–1991) have been observed in previous studies [Laštovička, 2019; Danilov, Vanina-Dart, 2010]. This issue is discussed in more detail in Subsection 1.3.

The first method of estimating the  $N_mF2$  trend approximates deviations of  $\Delta N_mF2$  from the multiple regression of  $N_mF2$  on  $F10.7$  and  $A_p$  by a linear time trend. When analyzing the trends, we have used two regressions on  $F10.7$  and  $A_p$ : (1) with the entire data set and (2) excluding years with  $F10.7 > 175$  s.f.u. Time variations in  $\Delta N_mF2$  and their approximations by linear time trends are illustrated in Figure 3.

The revealed trend is seen to be negative in all the cases, which indicates that  $N_mF2$  decreased from 1955 to 2021. Negative trends in  $N_mF2$  are consistent with the main results of the review [Danilov, Konstantinova,

2020] (this issue is discussed in more detail in Subsection 1.3). Note that the identified trends slightly reduce deviations from regressions on  $F10.7$ . The trend range is  $\sim 10$  times wider than the range of deviations from regressions for all the years and  $\sim 4$  times wider than the range of deviations from regressions for the years with  $F10.7 < 175$  s.f.u. In both cases, trend subtraction slightly reduces the standard deviation.

Table 1 lists the obtained coefficients of multiple regressions of  $N_mF2$  on  $F10.7$  and  $A_p$  ( $N_0$ ,  $N_1$ ,  $N_2$ ), as well as the trend rate of  $\Delta N_1$  for day, night, all years, and years with  $F10.7 < 175$  s.f.u. The exclusion of years with  $F10.7 > 175$  s.f.u. is seen to produce a noticeable change in the coefficients. For daytime conditions,  $N_0$  decreases by  $\sim 7\%$ ,  $N_1$  increases by  $\sim 6\%$ ,  $N_2$  decreases by  $\sim 78\%$  (i.e.  $\sim 4.5$  times), and  $\Delta N_1$  decreases by  $\sim 25\%$ . For nighttime conditions,  $N_0$  decreases by  $\sim 4\%$ ,  $N_1$  increases by  $\sim 4\%$ ,  $N_2$  decreases by  $\sim 43\%$  (i.e.  $\sim 1.8$  times), and  $\Delta N_1$  increases by  $\sim 13\%$ .

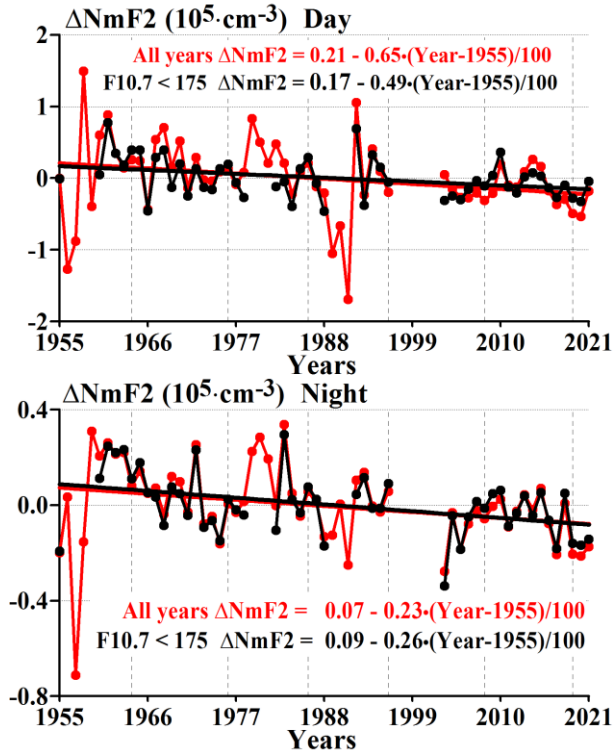


Figure 3. Time variations in  $\Delta N_m F2$  and their approximations by linear time trends for daytime (a) and nighttime (b). Red color indicates all years; black, years with  $F10.7 < 175$  s.f.u. Vertical dashed lines are boundaries between solar cycles

Table 1

Coefficients of regression on  $F10.7$  and  $A_p$  ( $N_0(10^5 \text{ cm}^{-3})$ ,  $N_1(10^5 \text{ cm}^{-3}/100 \text{ s.f.u.})$ ,  $N_2(10^5 \text{ cm}^{-3}/10 \text{ nT})$ , as well as the rate of trend  $\Delta N_1(10^5 \text{ cm}^{-3}/100 \text{ years})$

Period/time of day	$N_0$	$N_1$	$N_2$	$\Delta N_1$
All years/day	3.75	8.70	-0.23	-0.65
Years with $F$ 10.7<175/day	3.50	9.19	-0.05	-0.49
All years/night	1.63	2.16	-0.07	-0.23
Years with $F$ 10.7<175/night	1.57	2.25	-0.04	-0.26

Table 2

Estimated contributions of  $F10.7$ ,  $A_p$ , and trend to  $N_m F2$

Period/time of day	$F10.7$	$A_p$	Trend
All years/day	14.1	-0.45	-0.43
Years with $F$ 10.7<175/day	14.9	-0.10	-0.32
All years/night	3.5	-0.14	-0.15
Years with $F10.7 < 175$ /night	3.6	-0.08	-0.17

To assess the contributions of solar, geomagnetic activity, and long-term trend, we can use the obtained coefficients and extreme changes of  $F10.7=163$  s.f.u.,  $A_p=20$  nT, and  $Y=66$  years over the period of interest, using the formula for multiple regression of  $N_m F2$  on  $F10.7$  and  $A_p$ , as well as the formula for linear trend approximation of  $\Delta N_m F2$ . Table 2 gives assessments of  $F10.7$ ,  $A_p$ , and the trend. The solar activity contribution is seen to exceed the geomagnetic activity contribution  $\sim 25$ – $150$  times and the trend contribution  $\sim 21$ – $46$  times. Note that exclusion of years with  $F 10.7 > 175$  leads to a significant decrease in  $N_2$  ( $\sim 4.5$  times for the day and

$\sim 1.8$  times for the night), whereas a change in  $\Delta N_1$  is much smaller ( $\sim 25\%$  for the day and  $\sim 13\%$  for the night). This allows us to assume that when using all years,  $N_2$  reflects not so much the geomagnetic activity contribution as an attempt to compensate for abnormally low  $N_m F2$  at the maxima of cycles 19 and 22. At the same time, the trend effect is more stable and in both cases exhibits a negative trend with comparable coefficients.

The second method for estimating the long-term trend in  $N_m F2$  involves analyzing cycle-to-cycle variations in the coefficients of simple regression of  $N_m F2$  on  $F10.7$  (Figure 4). As expected, the coefficients for cycles 19 and 22 differ markedly from the coefficients obtained for other cycles. Under daytime conditions,  $N_0$  for cycles 19 and 22 is  $\sim 3.9 \cdot 10^5 \text{ cm}^{-3}$ ;

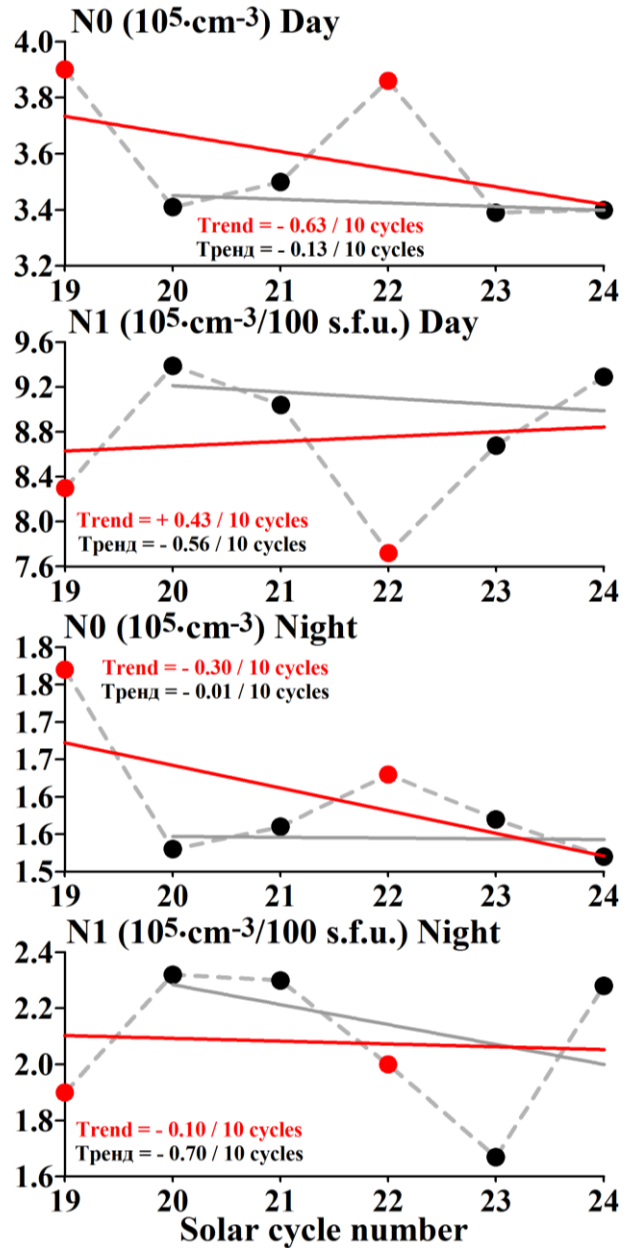


Figure 4. Cycle-to-cycle variations in coefficients of simple regression of  $N_m F2$  on  $F10.7$  for daytime (a, b) and nighttime (c, d). Red dots denote cycles 19 and 22; black dots mark the remaining cycles. The red trend is plotted for all cycles; the gray trend, for cycles 20, 21, 23, and 24



for other cycles, it varies within  $(3.4\div 3.5)\cdot 10^5 \text{ cm}^{-3}$ ;  $N_1$  for cycles 19 and 22 is  $8.3$  and  $7.7\cdot 10^5 \text{ cm}^{-3}/100 \text{ s.f.u.}$ ; for other cycles, it varies from  $8.7$  to  $9.4\cdot 10^5 \text{ cm}^{-3}/100 \text{ s.f.u.}$  Under daytime conditions, the linear trends, plotted for the coefficients of cycles 20, 21, 23, and 24, are as follows:  $N_0 = -0.13\cdot 10^5 \text{ cm}^{-3}/10 \text{ cycles}$  and  $N_1 = -0.56\cdot 10^5 \text{ cm}^{-3}/100 \text{ s.f.u.}/10 \text{ cycles}$ . To assess the trend contributions of the coefficients to the  $N_m F2$  trend, we employ the formula for simple regression of  $N_m F2$  on  $F10.7$ :  $N_m F2 \text{ trend} = N_0 \text{ trend} + N_1 (<F10.7> - 69)/100 \text{ trend}$ , where  $<F10.7> = 122 \text{ s.f.u.}$  is  $F10.7$  averaged over all the cycles being analyzed. The estimated trend  $N_m F2 = -0.43\cdot 10^5 \text{ cm}^{-3}/10 \text{ cycles}$  is close to the estimate obtained by the first method:  $\Delta N_1 = -0.49\cdot 10^5 \text{ cm}^{-3}/100 \text{ years}$  (10 cycles is approximately equivalent to 110 years). For nighttime conditions, a similar method gave a trend  $N_0 = -0.01\cdot 10^5 \text{ cm}^{-3}/10 \text{ cycles}$ , a trend  $N_1 = -0.70\cdot 10^5 \text{ cm}^{-3}/100 \text{ s.f.u.}/10 \text{ cycles}$ , and estimated trend  $N_m F2 = -0.38\cdot 10^5 \text{ cm}^{-3}/10 \text{ cycles}$ . This estimate significantly exceeds  $\Delta N_1 = -0.26\cdot 10^5 \text{ cm}^{-3}/100 \text{ years}$  for nighttime conditions. The reason for this difference is associated with overestimated nighttime trend in  $N_1$  due to abnormally low  $N_1$  in cycle 23 (the reasons may be related to the lack of data in this cycle).

### 1.3. Discussion of long-term variations in annual average $N_m F2$

Analysis of long-term variations in annual average  $N_m F2$  has revealed abnormally low  $N_m F2$  in 1957–1958 (maximum of cycle 19) and 1989–1991 (maximum of cycle 22). For daytime, the most abnormal is 1991 when the deviation from regression was  $-2.5\cdot 10^5 \text{ cm}^{-3}$  or  $-16\%$  of the expected value. For nighttime, the most abnormal is 1957,  $-0.85\cdot 10^5 \text{ cm}^{-3}$  or  $-16\%$  of the expected value. Analysis of the cycle-to-cycle variations in the coefficients of simple regression of  $N_m F2$  on  $F10.7$  has shown an abnormally low rate of change in  $N_m F2$  with increasing  $F10.7$  ( $N_1$ ) in the cycles considered. In cycle 22, this coefficient turned out to be  $15\%$  lower than  $N_1$ , derived by averaging over cycles 20, 21, 23, and 24. The fact that  $N_m F2$  near the maximum of cycle 21 (1979–1981) fits well into the regression curve plotted for the years with  $F10.7 < 175 \text{ s.f.u.}$  (i.e. without  $N_m F2$  near the maximum of cycle 21) suggests that the reason for the deviation from the regression in cycles 19 and 22 is not related to high solar activity per se.

The deviation from the regression curves near the maximum of solar cycle 22 (1989–1991) has been observed in previous studies. Laštovička [2019] has found that the rate of increase in annual average  $f_o F2$  and  $f_o E$  with increasing  $F10.7$  was higher in 1996–2014 (cycles 23 and 24) than in 1976–1995 (cycles 21 and 22). Noting that the mechanism of this difference has not been identified yet, Laštovička [2019] has put forward two potential reasons for this difference: (1) change in the ratio between  $F10.7$  and solar ionizing radiation; (2) change in the ratio between ionospheric parameters and solar ionizing radiation. The second reason may be linked to variations in the neutral atmosphere parameters (temperature, chemical composition, wind). Danilov

and Vanina-Dart [2010] have found that the deviation from the moving 11-year regression of  $f_o F2$  (at sunset)/ $f_o F2$  (14 LT) on  $F10.7$  begins to increase after 1980, peaking at the maximum of solar cycle 22. A change in the wind regime in the thermosphere was taken as a possible reason for the detected increase. Identifying the reason for the deviation from regression in cycles 19 and 22 (solar or atmospheric) is an urgent problem since other deviations from regression (including the long-term trend) can be explained by the same reason.

The use of alternative solar activity indices [Laštovička, Burešová, 2023] has shown that the difference between rates of increase in annual average  $f_o F2$  with increasing index in 1996–2014 and 1976–1995 depends essentially on the choice of solar activity index. For  $F10.7$  and the sunspot number, the difference was maximum; for the indices  $L\alpha$  (solar flux in the Lyman-alpha line),  $MgII$ , and  $HeII$ , it was smaller; and for  $F30$ , it was minimum. Thus, the results obtained in [Laštovička, Burešová, 2023] have confirmed the first version [Laštovička, 2019]: the reason for the anomaly at the maximum of cycle 19 is a change in the ratio between  $F10.7$  and solar ionizing radiation. In turn, the reason for the change in this ratio at the maximum of cycle 19 remains unclear so far.

The regression analysis has identified a negative trend in annual average  $N_m F2$ : under daytime conditions,  $N_m F2$  decreases at a rate of  $0.49\cdot 10^5 \text{ cm}^{-3}$  over 100 years or by  $0.32\cdot 10^5 \text{ cm}^{-3}$  over the 66-year period considered. As for average  $N_m F2$ , the trend rate is  $\sim 8\%$  over 100 years or a decrease by  $\sim 5\%$  over the 66-year period of interest. For nighttime conditions, a negative trend has also been found: the trend rate was  $0.26\cdot 10^5 \text{ cm}^{-3}$  over 100 years (or  $\sim 11\%$  relative to average  $N_m F2$ ). Given the quadratic dependence of  $N_m F2$  on  $f_o F2$ , the  $N_m F2$  trend can be recalculated into the  $f_o F2$  trend:  $\Delta f_o F2 / <f_o F2> \approx 0.5 \Delta N_m F2 / <N_m F2>$ , where parentheses mean averages over the 66-year period. The recalculation yields  $f_o F2$  trends:  $-0.26 \text{ MHz}$  over 100 years during the day and  $-0.23 \text{ MHz}$  over 100 years at night.

The obtained trends in  $N_m F2$  and  $f_o F2$  were compared with the trends presented in the review [Danilov, Konstantinova, 2020]. On the one hand, the authors show small  $f_o F2$  trends from  $-0.0028$  to  $-0.0002 \text{ MHz}$  per year (from  $-0.28$  to  $-0.02 \text{ MHz}$  over 100 years) [Bremer et al., 2012; Mielich, Bremer, 2013]. The largest trend from the presented range agrees well with the results of our work. On the other hand, the review presents the trends that are several times or even an order of magnitude higher than those we have obtained. The results of the analysis of  $f_o F2$  trends in [Cnossen, Franzke, 2014] show that all statistically significant  $f_o F2$  trends are negative, and their absolute values range from  $0.008$  to  $0.033 \text{ MHz/year}$  (the latter value is more than by an order of magnitude higher than the trend we have estimated). Zhang [2018] has presented electron density trends in the F-region from incoherent scatter data. According to the data, the  $N_m F2$  trend is  $5\%$  per decade, which is  $\sim 5$ – $6$  times higher than the  $N_m F2$  trend we have estimated ( $8$ – $11\%$  for 100 years).

Given that the range of the  $N_mF2$  or  $f_oF2$  trend is much narrower than the range of deviations from regression, the discrepancies between the small trends are quite understandable. At the same time, it is difficult to explain the trends that are several times or even by an order of magnitude higher than those we have derived. For example, the  $N_mF2$  trend equivalent to 5 % over a decade would give a change of  $\sim 33$  % in regression coefficients over six cycles, which would be visible to the naked eye. We have shown that the cycle-to-cycle variation in regression coefficients can be  $\sim 15$  %, yet such a variation is not a trend, but an anomaly in a certain cycle.

## 2. YEAR-TO-YEAR VARIATIONS IN $N_mF2$ , $T_m$ , AND THEIR VARIABILITIES IN SOLAR CYCLE 24

### 2.1. Data and analysis method

The analysis uses experimental data on the OH rotational temperature  $T_m$  (OH band(6-2) 834.0 nm,  $\sim 87$  km), derived from spectrometric measurements at the ISTP SB RAS Geophysical Observatory (51.8° N, 103.1° E, Tory) with 10 min resolution, and the peak electron density  $N_mF2$ , obtained from vertical sounding data by the Irkutsk digisonde DPS-4 (52.3° N, 104.3° E) operating in monitoring mode with 15 min resolution. Measuring and data processing techniques are detailed in [Semenov, et al., 2002; Khomich et al., 2008; Medvedeva et al., 2014]. The OH rotational temperature displays the temperature of the atmosphere at the mesopause; the period of interest is 2008–2020. For each year, we have calculated annual average  $T_m$  and  $N_mF2$  and their variabilities  $\sigma T_m$  and  $\sigma N_mF2$ . The analysis involves data on  $F10.7$  and  $A_p$  from the GSFC/SPDF OmniWeb interface on the website [<http://omniweb.gsfc.nasa.gov/form/dx1.html>], as well as data on  $SOI$  variations in the format of the Climatic Research Unit of East Anglia University [<https://crudata.uea.ac.uk/cru/data/soi/>, Ropelewski, Jones, 1987]. Negative values of this index indicate an El Niño phase; positive values, a La Niña phase. The El Niño — Southern Oscillation (ENSO) is the main climatic signal that determines the year-to-year variability in the global ocean—atmosphere system. We have studied and compared annual average  $T_m$  and  $N_mF2$ , as well as their day-to-day and intradiurnal variabilities, calculated using the method presented in [Medvedeva, Ratovsky, 2017].

To calculate annual average  $T_m$  and  $\sigma T_m$  for each year, we have adopted the method detailed in [Offermann et al., 2009; Perminov et al., 2014a, b; Medvedeva, Ratovsky, 2015, 2017]. As a characteristic of atmospheric variability, we have used standard deviations of  $T_m$  in annual and nighttime variations, which allow us to analyze the manifestation of wave processes of various time scales in the upper atmosphere. Day-to-day temperature variations are generally caused by migrating planetary waves; the main contribution to the nighttime variability is made by tides and IGWs. The time period 2008–2020 includes 2185 nights of observations. To determine average  $T_m$  and day-to-day  $\sigma T_m$ , we

isolated seasonal variations from the set of averages for each night of observations, and then analyzed temperature residuals. Seasonal variations were computed using the least square method:

$$T = \bar{T} + \sum_{n=1}^3 A_n \cos\left(\frac{2\pi n}{365.25}(t_d - \varphi_n)\right), \quad (1)$$

where  $\bar{T}$  is the annual average temperature,  $t_d$  is the day of the year,  $A_n$  and  $\varphi_n$  are  $n$  harmonic amplitudes and phases. The approximation was carried out by the sum of the first three harmonics of the seasonal variation with periods of 12, 6, and 4 months.

The main contribution to the nighttime variability in  $T_m$  is made by tides and IGWs. Intradiurnal temperature variations were analyzed using the method described in [Offermann et al., 2009, Perminov et al., 2014a, b; Medvedeva, Ratovsky, 2015]: the square of this standard deviation can be represented as the sum of squared standard deviations

$$\sigma^2 = \sigma_{td}^2 + \sigma_{gw}^2 + \sigma_n^2 \quad (2)$$

characterizing activity during the night of tides  $\sigma_{td}^2$ , IGW  $\sigma_{gw}^2$ , as well as fluctuations in the dark current of the spectrometer receiver  $\sigma_n^2$ , which are determined when the entrance slit of the device is closed. The values  $\sigma_{gw}$  and  $\sigma_{td}$  were sequentially calculated after isolating the harmonics corresponding to the 24, 12, and 8 hr diurnal tide components from a series of nighttime temperatures by the least square method. This procedure was carried out for each night of observations. The  $\sigma_{td}$  and  $\sigma_{gw}$  thus calculated were utilized as parameters describing temperature variability due to tides and IGWs.

As a characteristic of ionospheric variability we used  $\sigma N_mF2$ . For the analysis, the relative disturbances  $\Delta N_mF2$  were calculated which represent the relative difference between observed  $N_mF2_{obs}$  and the moving 27-day median  $N_mF2_{med}$ :

$$\Delta N_mF2 = (N_mF2_{obs} - N_mF2_{med}) / N_mF2_{med} \cdot 100\%. \quad (3)$$

Root-mean-square  $\Delta N_mF2$  was chosen as the parameter of ionospheric variability:

$$\sigma N_mF2 = \sqrt{\langle \Delta N_mF2^2 \rangle}. \quad (4)$$

The obtained values of  $\Delta N_mF2$  were analyzed in the same time periods as  $T_m$ ; to do this, we isolated wave disturbances with  $T > 24$ ,  $8 \leq T \leq 24$ , and  $T < 8$  hrs. The values of  $\Delta N_mF2$  were analyzed separately for daytime and nighttime; the day–night boundary was determined from the passage of the terminator across the earth. Day-to-day ( $T > 24$  hrs) variations in  $N_mF2$  can be caused by geomagnetic disturbances, planetary waves, as well as short-term solar activity variations. Variations with periods  $8 \leq T \leq 24$  hrs correspond to the first three harmonics of thermal tides (24, 12, and 8 hrs) and can be triggered by tidal waves from the underlying atmosphere and by geomagnetic storms. The most rapid variations ( $T < 8$  hrs) are associated with traveling ionospheric disturbances (TIDs), which can be generated by IGWs propagating from the lower layers.

Variabilities in  $T_m$  and  $N_mF2$  corresponding to different periods are further designated as day-to-day ( $T > 24$  hrs), tidal ( $8 \leq T \leq 24$  hrs), and IGW ( $T < 8$  hrs) variabilities.

To analyze year-to-year variations of ionospheric variability in  $\sigma N_mF2$  and their relationship with solar and geomagnetic activity variations, we have performed multiple regression analysis between  $\sigma N_mF2$  and annual average  $F10.7$  and  $A_p$ . The equation for multiple regression of  $\sigma N_mF2$  on  $F10.7$  and  $A_p$  has the form

$$\sigma N_mF2 = \sigma_0 + \sigma_F (F10.7 - 69)/10 + \sigma_A (A_p - 4), \quad (5)$$

where  $\sigma_0$  is the regression constant at  $F10.7=69$  s.f.u. and  $A_p=4$  nT;  $\sigma_F$  and  $\sigma_A$  are regression slopes indicating the rate of change in  $\sigma N_mF2$  with increasing  $F10.7$  and  $A_p$  respectively. The constant  $\sigma_0$  fits solar-geomagnetic conditions during the deep solar minimum of 2009 ( $F10.7=69$  s.f.u.,  $A_p=4$  nT).

The coefficient of determination is an important characteristic of any regression. For multiple regression of  $\sigma N_mF2$  on  $F10.7$  and  $A_p$ , the coefficient of determination indicates what percentage (%) of year-to-year variations  $\sigma N_mF2$  can be explained by concurrent variations in solar and geomagnetic activity ( $F10.7$  and  $A_p$ ). In the case of a simple regression on  $F10.7$  or  $A_p$ , the coefficient of determination shows how much the  $\sigma N_mF2$  variation can be explained by variations only in solar or geomagnetic activity (only  $F10.7$  or  $A_p$ ). For the analysis of  $N_mF2$  variations, we employed multiple regressions of  $\sigma N_mF2$  and annual average  $N_mF2$  on  $F10.7$  and  $A_p$ , as well as simple regressions on  $F10.7$  and  $A_p$ . To study  $\sigma T_m$ , we adopted the same procedure and additionally included  $SOI$  in the analysis.

## 2.2. Results of the analysis of year-to-year variations in the peak electron density and its variability in solar cycle 24 and their discussion

Figure 5, *a* illustrates year-to-year variations in annual average  $N_mF2$  (circles) with the linear regression results superimposed on annual average  $F10.7$  for daytime (black, gray) and nighttime (blue, light blue) conditions. Panel *b* exhibits variations in  $F10.7$  (black curve) and  $A_p$  (blue curve).

The  $F10.7$  variations are seen to be ahead of the  $A_p$  variations by  $\sim 1$  year during the increase phase and by  $\sim 2$  years during the declining phase. The analysis has shown that the regression of annual average  $N_mF2$  on  $F10.7$  is almost perfect, and the asymmetry of solar and geomagnetic activity variations did not worsen the regression. Calculations have revealed that the coefficient of determination for the simple linear regression of annual average  $N_mF2$  on  $F10.7$  is very high (99.5 % for daytime and 98 % for nighttime). This means that the contribution of geomagnetic activity to year-to-year variations in annual average  $N_mF2$  for 2008–2020 is negligible compared to the contribution of solar activity.

Figure 6 depicts year-to-year variations in  $\sigma N_mF2$  and their approximation by multiple regression on  $F10.7$  and  $A_p$ . Table 3 lists determination coefficients for the multiple regression  $R_{FA}^2$  calculated from (5), the simple regression  $R_F^2$  on  $F10.7$ , and the simple regression  $R_A^2$  on  $A_p$ .

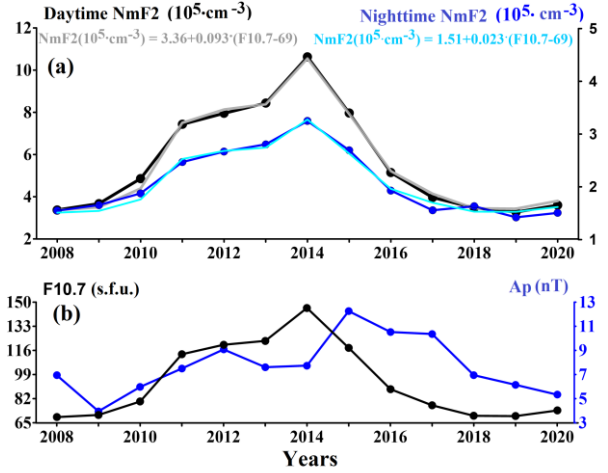


Figure 5. Variations in annual average  $N_mF2$  (circles) with linear regression results superimposed on annual average  $F10.7$  for daytime (black, gray) and nighttime (blue, light blue) conditions (*a*); year-to-year variations in  $F10.7$  (black) and  $A_p$  (blue) in solar cycle 24 (*b*)

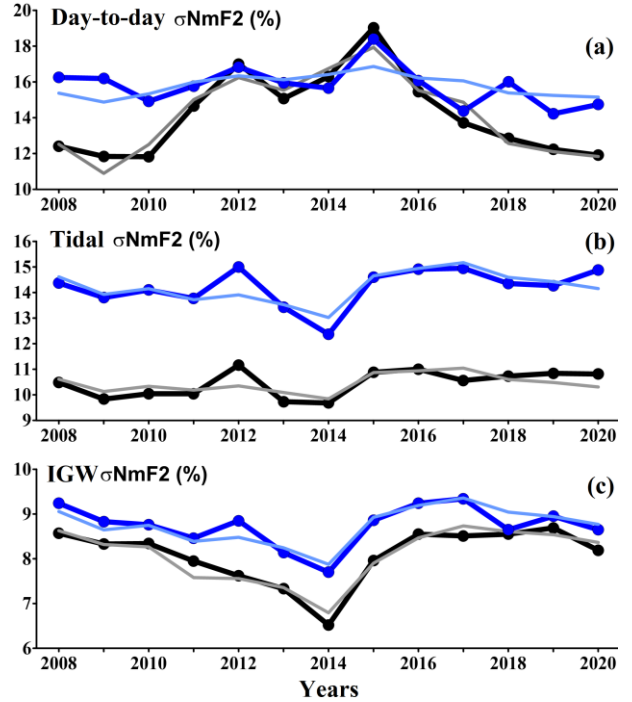


Figure 6. Year-to-year variations in  $\sigma N_mF2$  (circles) and their approximation by multiple regression on  $F10.7$  and  $A_p$  for daytime (black, gray) and nighttime (blue, light blue) conditions: *a* — day-to-day variability; *b* — with tidal periods; *c* — with IGW periods

The multiple regression has been found to significantly increase the coefficient of determination as compared to the simple regression for four of the six variability types; in Table 3, these values are highlighted in bold with underscore. Thus, the coefficient of determination increases from 66 to 92 % for daytime day-to-day  $N_mF2$ , from 19 to 48 % for day-to-day tidal  $\sigma N_mF2$ , from 27 to 65 % for nighttime tidal  $\sigma N_mF2$ , and from 48 to 83 % for nighttime  $\sigma N_mF2$  with IGW periods. This indicates that the solar and geomagnetic activity contributions to ionospheric variability of these types are comparable.



Table 3  
Determination coefficients for multiple  $R_{FA}^2$  and simple regressions  $R_F^2, R_A^2$  of ionospheric variability  $\sigma N_m F2$  on  $F10.7$  and  $A_p$

Variability $\sigma N_m F2$	$R_{FA}^2, \%$	$R_F^2, \%$	$R_A^2, \%$
Day-to-day	Day <b>91.9</b>	65.6	66.0
Tidal	<b>48.0</b>	8.8	19.1
IGW	92.6	83.2	1.3
Day-to-day	Night 29.6	19.1	23.1
Tidal	<b>64.6</b>	27.4	10.6
IGW	<b>82.7</b>	47.7	5.6

For daytime  $\sigma N_m F2$  with IGW periods the coefficient of determination for the simple regression on  $F10.7$  is 83 %, and the multiple regression gives an increase of 10 %, which suggests that the solar activity contribution dominates. For nighttime day-to-day  $\sigma N_m F2$ , none of the regressions yields a coefficient of determination  $>30$  %, which indicates a small contribution of both solar and geomagnetic activity.

Thus, the regression analysis has demonstrated that there is a positive correlation of daytime day-to-day  $\sigma N_m F2$  with both solar and geomagnetic activity, which was expected since diurnal solar flux variations and geomagnetic storms increase ionospheric variability. For daytime day-to-day variability, the coefficient of determination increases from 66 % for simple regression of  $\sigma N_m F2$  on  $A_p$ , to 92 % for multiple regression of  $\sigma N_m F2$  on  $F10.7$  and  $A_p$ , which can be attributed to the comparability of the effects of geomagnetic and solar activity on  $\sigma N_m F2$ . The comparability of geomagnetic and solar activity contributions to  $N_m F2$  variability is inconsistent with the results obtained in [Forbes et al., 2000; Rishbeth, Mendillo, 2001]; the authors have concluded that variability in the ionosphere due to day-to-day variations in solar activity is lower than that in geomagnetic activity. This discrepancy can be explained by two reasons. First, in solar cycle 24, geomagnetic activity was atypically low. Rishbeth and Mendillo [2001] have utilized  $A_p=13$  nT as typical (or moderate) geomagnetic activity, whereas in cycle 24 the highest annual average  $A_p=12.3$  nT, which is  $\sim 1.8$  times lower than in solar cycle 23. Another reason can be different methods of estimating solar and geomagnetic activity contributions. Forbes et al. [2000] have employed multiple regression of daily average  $N_m F2$  by the annual component of variations, the semiannual component of variations,  $F10.7$  averaged over 81 days, and day-to-day  $F10.7$ . It was the last regression component that was used to assess the contribution of day-to-day variations in solar activity to  $\sigma N_m F2$ . Unlike [Forbes et al., 2000], we have analyzed multiple regression of  $\sigma N_m F2$  on  $F10.7$  and  $A_p$ . Currently, it is difficult to say which method is more valid, but the following conclusion can be drawn. If the geomagnetic activity contribution had been dominant, we would not have received a significant increase in the coefficient of determination for the multiple regression on  $F10.7$  and  $A_p$  as compared to the

simple regression on  $A_p$ .

Regression analysis has shown a positive correlation of nighttime day-to-day  $\sigma N_m F2$  with both solar and geomagnetic activity; however, sensitivity to geomagnetic/solar activity was  $\sim 3-4$  times lower than for daytime variability. Such low sensitivity leads to a low coefficient of determination, which indicates that only  $\sim 30$  % of year-to-year variations in nighttime and diurnal  $\sigma N_m F2$  can be explained by simultaneous variations in solar and geomagnetic activity. The absence of an increase in nighttime variability with geomagnetic activity or even its decrease have been observed in a number of previous studies [Ratovsky et al., 2015; Altadill, 2007; Mikhailov et al., 2000; Araujo-Pradere et al., 2005; Deminov et al., 2013]. Among the reasons explaining this behavior, the authors pointed to the increase in chemical control (or recombination rate) with increasing geomagnetic activity, which reduced the amplitude of nighttime disturbances of  $N_m F2$ . Another reason may be related to nighttime disturbances of  $N_m F2$  triggered by so-called CIR storms (storms initiated by a compression region in front of high-speed streams) [Buresova et al., 2014; Ratovsky et al., 2022]. CIR storms can occur at low  $A_p$  and can enhance nighttime  $\sigma N_m F2$  during geomagnetic minima. For geomagnetic activity of this kind,  $A_p$  cannot be a suitable indicator. In this case, the coefficient  $\sigma_0$  in (5) includes contributions from both meteorological and geomagnetic activity, which is not identified with  $A_p$ .

### 2.3. Results of the analysis of year-to-year variations in $T_m$ and $\sigma T_m$ in solar cycle 24 and their discussion

Initially, multiple linear regressions of  $T_m$  and  $\sigma T_m$  on  $F10.7$  and  $A_p$  were plotted in the same way as it was done for  $N_m F2$  according to (5). Unlike  $N_m F2$ , no significant relationship with  $F10.7$  and  $A_p$  was found in variations of annual average  $T_m$  and  $\sigma T_m$ . It was then decided to involve an additional parameter describing conditions of the lower atmosphere in the analysis, for which  $SOI$  was chosen. Analysis of multiple regression of  $T_m$  and  $\sigma T_m$  on  $SOI$  and  $F10.7$  (7), as well as  $T_m$  and  $\sigma T_m$  on  $SOI$  and  $A_p$  (6) was carried out and the determination coefficients for regression of each type were calculated.

$$\sigma T_m = \sigma_0 + \sigma_S SOI + \sigma_A (A_p - 4), \quad (6)$$

$$\sigma T_m = \sigma_0 + \sigma_S SOI + \sigma_F (F10.7 - 69)/10. \quad (7)$$

Figure 7 depicts year-to-year variations in mesopause temperature variability  $\sigma T_m$  and their approximations by multiple regression on  $SOI$  and  $A_p$  ( $a-c$ ), variations in annual average  $T_m$  and their approximation by multiple regression on  $SOI$  and  $F10.7$  ( $d$ ), as well as variations in annual average  $SOI$  ( $e$ ). Analysis of multiple regression of  $\sigma T_m$  on  $SOI$  and  $F10.7$ , as well as of  $\sigma T_m$  on  $SOI$  and  $A_p$ , has shown that the highest determination coefficients were obtained for multiple regression on  $SOI$  and  $A_p$ ; the approximation results are presented in Figure 7 ( $a-c$ ).

Table 4 lists determination coefficients for multiple ( $R_{FA}^2$ ) and simple ( $R_F^2, R_A^2$ ) regressions of  $\sigma T_m$  on  $F10.7$  and  $A_p$ , as well as for multiple regression of  $\sigma T_m$  on  $SOI$



and  $A_p$  ( $R_{SA}^2$ ). It has been found that the inclusion of  $SOI$  in the analysis significantly improves the quality of approximation, which can indicate that the El Niño/La Niña phenomena have an effect on parameters of the mid-latitude upper atmosphere. Compared to the regression

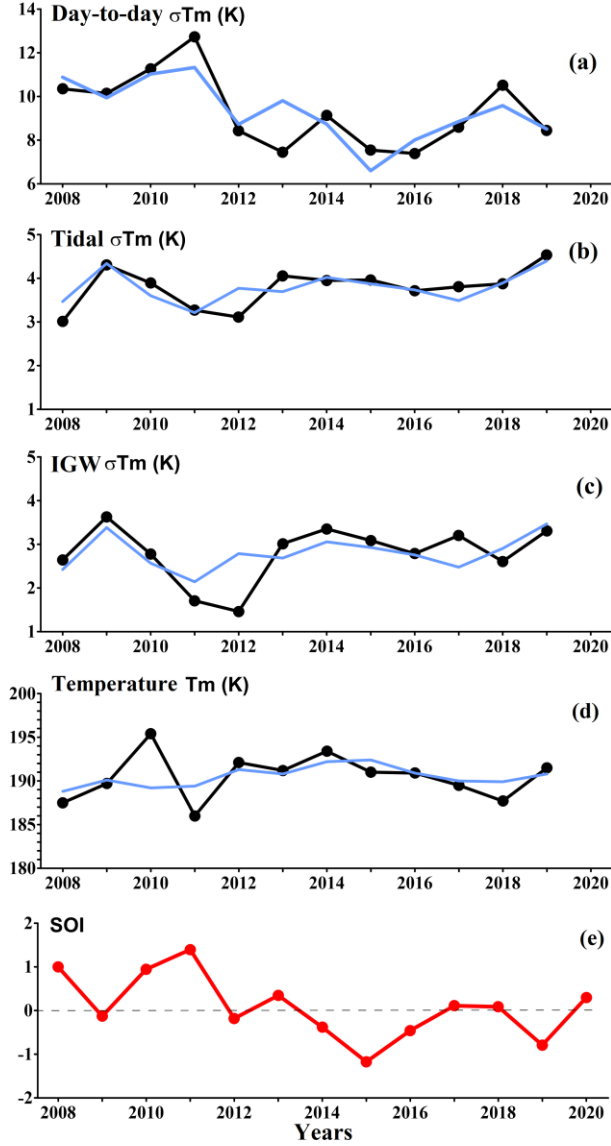


Figure 7. Year-to-year variations in  $\sigma T_m$  (black curve) and their approximations by multiple regression on  $SOI$  and  $A_p$  (blue curve): *a* — day-to-day variability; *b* — with tidal periods; *c* — with IGW periods; *d* — variations in annual average  $T_m$  (black curve) and their approximation by multiple regression on  $SOI$  and  $F10.7$  (blue curve); *e* — variations in annual average  $SOI$

Table 4

Determination coefficients for multiple ( $R_{FA}^2$ ) and simple ( $R_F^2$ ,  $R_A^2$ ) regressions of  $\sigma T_m$  on  $F10.7$  and  $A_p$ , as well as for multiple regression of  $\sigma T_m$  on  $SOI$  and  $A_p$  ( $R_{SA}^2$ )

Type of variability $T_m$	$R_{FA}^2$ %	$R_F^2$ %	$R_A^2$ %	$R_{SA}^2$ %
Day-to-day	32.2	5.9	32.2	66.7
Tidal	7.0	2.6	6.6	56.8
IGW	6.2	5.3	3.1	35.5

of  $\sigma T_m$  on  $F10.7$  and  $A_p$ , the coefficients of determination increase significantly from  $\sim 32$  to 67 % for day-to-day  $\sigma T_m$ , from  $\sim 7$  to 57 % for tidal  $\sigma T_m$ , and from  $\sim 6$  to 36 % for  $\sigma T_m$  with IGW periods. Day-to-day  $\sigma T_m$ , driven by the influence of migrating planetary waves, correlates with  $SOI$ , with a peak of variability in the La Niña phase (maximum  $SOI$  in 2011), and a minimum in the El Niño phase. Intradiurnal variability generated by tides and IGWs (Figure 7, *b*, *c*) demonstrates a negative correlation with  $SOI$ ; the lowest variability is observed near the La Niña phase (2011–2012).

Pedatella and Liu [2012] have made numerical calculations with WACCM (Whole Atmosphere Community Climate Model) and have shown that the El Niño — Southern Oscillation (ENSO) can cause significant year-to-year variability in migrating and nonmigrating tides in the mesosphere and lower thermosphere region (MLT). The authors have concluded that the tides exhibit the greatest response to ENSO. Pedatella and Liu [2013] have concluded that ENSO can be considered as a potentially significant source of variability in the upper atmosphere. Thus, the observed increase in intradiurnal temperature variability of the mesopause region during the El Niño phase may be associated with intensification of tidal waves in the upper atmosphere. Analysis of day-to-day  $\sigma T_m$ , determined by migrating planetary waves, has revealed its correlation with  $SOI$  variations, with maximum variability during the La Niña phase (maximum  $SOI$  in 2011), and minimum variability during the El Niño phase (Figure 7, *a*). This contradicts the conclusion drawn in [Pedatella, Liu, 2013; Sassi et al., 2004] that a significant increase in activity of planetary waves occurs during El Niño. Pedatella and Liu [2013] from model calculations have concluded that at low latitudes during El Niño westward abnormal zonal-mean winds occur in the altitude range 40–60 km; and eastward ones, at 60–90 km. The opposite situation is observed during the La Niña phase. Sassi et al. [2004] have also revealed that ENSO causes the low-latitude stratosphere and mesosphere to vary. Nonetheless, García-Herrera et al. [2006] did not find significant variability in atmospheric parameters at low latitudes. A possible reason for this discrepancy may be linked to the use of different models in [Pedatella, Liu, 2013; Sassi et al., 2004; García-Herrera et al., 2006], as well as to the choice of ENSO events for analysis. In [Offermann et al., 2009; Perminov et al., 2014a, b], differences in  $\sigma T_m$  have been found for different regions. We can assume that the reason for the discrepancy between our result (an increase in day-to-day  $\sigma T_m$  during the La Niña phase) and the conclusions drawn in [Pedatella, Liu, 2013; Sassi et al., 2004] (an increase in the activity of planetary waves during the El Niño phase) may be latitude and longitude differences between the regions considered.

Analysis of multiple regression of annual average  $T_m$  on  $F10.7$  and  $A_p$  has not revealed their significant correlation (coefficient of determination is 9.1 %). The best coefficient of determination (18.1 %) is obtained from multiple regression of annual average  $T_m$  on  $SOI$  and  $F10.7$ . The results of the analysis are presented in Figure 7, *d*.

Low coefficients of determination are associated with the behavior of the annual average mesopause temperature in 2009–2011: none of the indices reproduces a sharp increase in 2009–2010 and a sharp decrease in 2010–2011. Sun et al. [2019] have examined the effect of the El Niño — Southern Oscillation on the total electron content (TEC) of the ionosphere and have shown that the contribution of the ENSO cold phase in 2010 and 2011 to quasi-biennial fluctuations in TEC variations is significant. A possible reason for the considerable variations in annual average  $T_m$  in 2009–2011 may be the cold phase of La Niña and the highest  $SOI$  values over the past 70 years (Figure 7, e).

To study the relationship between  $\sigma T_m$  and  $\sigma N_m F2$ , we calculated the correlation and determination coefficients between the year-to-year variations in these characteristics at night. The calculations found out that there was a low negative correlation with coefficients of  $-0.229$  for day-to-day variability,  $-0.284$  for tidal variability, and  $-0.046$  for variability with IGW periods. The corresponding determination coefficients were 5.2, 8.1, and 0.2 %. Thus, no significant relationship was found between year-to-year variations in  $\sigma T_m$  and  $\sigma N_m F2$  at night. Comparison between year-to-year variations in  $\sigma N_m F2$  and  $SOI$  also revealed no significant relationship between these characteristics.

## CONCLUSION

The study of long-term variations in annual average  $N_m F2$  over the 66-year period has led to the following conclusions.

The main factor of variations in the annual average daytime and nighttime values is solar activity variation (determination coefficients of 98 % during the day and 97 % at night). Taking geomagnetic activity into account has practically no effect on regression errors. Approximation of deviations from the  $\Delta N_m F2$  regression by a linear time trend has found negative trends in long-term variations of  $N_m F2$ :  $0.49 \cdot 10^5 \text{ cm}^{-3}/100$  years during the day and  $0.26 \cdot 10^5 \text{ cm}^{-3}/100$  years at night. The trend range is  $\sim 10$  times narrower than the range of deviations from regressions for all years and  $\sim 4$  times narrower than the range of deviations from regressions for years with  $F10.7 < 175$  s.f.u. In both cases, trend subtraction slightly reduces the standard deviation. The greatest deviations from the regressions on  $F10.7$  are observed in the years near maxima of solar cycles 19 and 22. This fact has been observed in previous studies, and the reason for the deviations is currently debatable. Comparison of the obtained trends in  $N_m F2$  with the trends presented in the review [Danilov, Konstantinova, 2020] has indicated that they agree with small trends in  $f_o F2$ ; at the same time, the review shows trends that are several times or even by an order of magnitude higher than those we have derived. The analysis has revealed that cycle-to-cycle variations in regression coefficients can be  $\sim 15$  %; yet, such a variation is not a trend, but an anomaly in a certain cycle.

Using radiophysical and spectrometric measurements at the ISTP SB RAS complex of instruments in solar cycle 24, we have studied year-to-year variations in  $N_m F2$ ,  $T_m$ , and their variability. As a result of multiple regression analysis, the following conclusions have been drawn. The main contribution to year-to-year variations

in annual average  $N_m F2$  is made by solar activity; the contribution of geomagnetic activity is negligible. For four of six types of ionospheric variability, the contributions of solar and geomagnetic activity are comparable. For daytime  $\sigma N_m F2$  with IGW periods, the influence of solar activity prevails. For nighttime day-to-day  $\sigma N_m F2$ , the contribution of both solar and geomagnetic activity is insignificant. Analysis of year-to-year variations in  $\sigma T_m$  has shown that the inclusion of  $SOI$  in the multiple regression analysis can cause a significant increase in the coefficients of determination: the highest were obtained for multiple regression on  $SOI$  and  $A_p$ . This may suggest that the El Niño/La Niña phenomena have an effect on characteristics of the mid-latitude upper atmosphere. Day-to-day  $\sigma T_m$  correlates with  $SOI$ , with peak variability during the La Niña phase (2011–2012). Maximum intra-diurnal  $\sigma T_m$  is observed near the El Niño phase. For annual average  $T_m$ , the highest coefficient of determination (18.1 %) is given by multiple regression on  $SOI$  and  $F10.7$ . No significant relationship has been found between year-to-year variations in  $\sigma N_m F2$  and  $\sigma T_m$ .

The research was financially supported by RSF (Grant No. 22-17-00146) [<https://rscf.ru/project/22-17-00146/>]. The analysis was based on experimental data from the Shared Equipment Center "Angara" [<http://ckp-rf.ru/ckp/3056/>], obtained with the financial support from the Ministry of Science and Higher Education of the Russian Federation.

## REFERENCES

- Altadill D. Time/altitude electron density variability above Ebro, Spain. *Adv. Space Res.* 2007, vol. 3, pp. 962–969. DOI: [10.1016/j.asr.2006.05.031](https://doi.org/10.1016/j.asr.2006.05.031).
- Araujo-Pradere E.A., Fuller-Rowell T.J., Codrescu M.V., Bilitza D. Characteristics of the ionospheric variability as a function of season, latitude, local time, and geomagnetic activity. *Radio Sci.* 2005, vol. 40, RS5009. DOI: [10.1029/2004rs003179](https://doi.org/10.1029/2004rs003179).
- Beig G. Long-term trends in the temperature of the mesosphere/lower thermosphere region: 2. Solar response. *J. Geophys. Res. Atmos.* 2011, vol. 116, A00H12. DOI: [10.1029/2011ja.016766](https://doi.org/10.1029/2011ja.016766).
- Bremer J. Trends in the ionospheric E and F regions over Europe. *Ann. Geophys.* 1998, vol. 16, no 8, pp. 986–996. DOI: [10.1007/s00585-998-0986-9](https://doi.org/10.1007/s00585-998-0986-9).
- Bremer J., Damboldt T., Mielich J., Suessmann P. Comparing long-term trends in the ionospheric F2 region with two different methods. *J. Atmos. Solar-Terr. Phys.* 2012, vol. 77, pp. 174–185. DOI: [10.1016/j.jastp.2011.12.017](https://doi.org/10.1016/j.jastp.2011.12.017).
- Bilitza D., Altadill D., Truhlik V., Shubin V., Galkin I., Reinisch B., Huang X. International Reference Ionosphere 2016: From ionospheric climate to real-time weather predictions. *Space Weather.* 2017, vol. 15, pp. 418–429. DOI: [10.1002/2016SW.001593](https://doi.org/10.1002/2016SW.001593).
- Buresova D., Laštovička J., Hejda P., Bochnicek J. Ionospheric disturbances under low solar activity conditions. *Adv. Space Res.* 2014, vol. 54, pp. 185–196. DOI: [10.1016/j.asr.2014.04.007](https://doi.org/10.1016/j.asr.2014.04.007).
- Cnossen I., Franzke C. The role of the Sun in long-term change in the F2 peak ionosphere: new insights from Ensemble Empirical Mode Decomposition (EEMD) and numerical modeling. *J. Geophys. Res.* 2014, vol. 119, no. 10, pp. 8610–8623. DOI: [10.1002/2014JA020048](https://doi.org/10.1002/2014JA020048).
- Danilov A.D., Vanina-Dart L.B. Comparison of  $f_o F2$  values in the daytime and after sunset. *Geomagnetism and Aeronomy.* 2010, vol. 50, no 1, pp. 58–63. DOI: [10.1134/S001679321001007X](https://doi.org/10.1134/S001679321001007X).

- Danilov A.D., Konstantinova A.V. Long-term variations in the parameters of the middle and upper atmosphere and ionosphere (review). *Geomagnetism and Aeronomy*. 2020, vol. 60, no 4, pp. 397–420. DOI: [10.1134/S0016793220040040](https://doi.org/10.1134/S0016793220040040).
- Deminov M.G., Deminova G.F., Zherebtsov G.A., Polekh N.M. Statistical properties of variability of the quiet ionosphere F2-layer maximum parameters over Irkutsk under low solar activity. *Adv. Space Res.* 2013, vol. 51, pp. 702–711. DOI: [10.1016/j.asr.2012.09.037](https://doi.org/10.1016/j.asr.2012.09.037).
- Drob D.P., Emmert J.T., Meriwether J.W., Makela J.J., Doornbos E., Conde M., Hernandez G., Noto J., Zawdie K.A., McDonald S.E., et al. An update to the Horizontal Wind Model (HWM): The quiet time thermosphere. *Earth and Space Sci.* 2015, vol. 2, pp. 301–319. DOI: [10.1002/2014EA000089](https://doi.org/10.1002/2014EA000089).
- Forbes J.M., Palo S.E., Zhang X. Variability of the ionosphere. *J. Atmos. Solar-Terr. Phys.* 2000, vol. 62, pp. 685–693. DOI: [10.1016/s1364-6826\(00\)00029-8](https://doi.org/10.1016/s1364-6826(00)00029-8).
- García-Herrera R., Calvo N., Garcia R.R., Giorgetta M.A. Propagation of ENSO temperature signals into the middle atmosphere: A comparison of two general circulation models and ERA-40 reanalysis data. *J. Geophys. Res.* 2006, vol. 111, D06101. DOI: [10.1029/2005JD006061](https://doi.org/10.1029/2005JD006061).
- Khomich V.Y., Semenov A.I., Shefov N.N. Airglow as an Indicator of Upper Atmospheric Structure and Dynamics, Springer: Berlin/Heidelberg, Germany, 2008.
- Laštovička J. Is the relation between ionospheric parameters and solar proxies stable? *Geophys. Res. Lett.* 2019, vol. 46, no. 24, pp. 14208–14213. DOI: [10.1029/2019GL085033](https://doi.org/10.1029/2019GL085033).
- Laštovička J., Burešová D. Relationships between  $f_oF2$  and various solar activity proxies. *Space Weather*. 2023, vol. 21, e2022SW003359. DOI: [10.1029/2022SW003359](https://doi.org/10.1029/2022SW003359).
- Medvedeva I., Ratovsky K. Studying atmospheric and ionospheric variabilities from long-term spectrometric and radio sounding measurements. *J. Geophys. Res.: Space Phys.* 2015, vol. 120, pp. 5151–5159. DOI: [10.1002/2015ja021289](https://doi.org/10.1002/2015ja021289).
- Medvedeva I.V., Ratovsky K.G. Comparative analysis of atmospheric and ionospheric variability by measurements of temperature in the mesopause region and peak electron density  $N_mF2$ . *Geomagnetism and Aeronomy*. 2017, vol. 57, pp. 217–228. DOI: [10.1134/s0016793217020104](https://doi.org/10.1134/s0016793217020104).
- Medvedeva I.V., Semenov A.I., Perminov V.I., Beletsky A.B., Tatarnikov A.V. Comparison of ground-based OH temperature data measured at Irkutsk (52° N, 103° E) and Zvenigorod (56° N, 37° E) stations with Aura MLS v3.3. *Acta Geophys.* 2014, vol. 62, pp. 340–349.
- Mielich J., Bremer J. Long-term trends in the ionospheric F2 region with two different solar activity indices. *Ann. Geophys.* 2013, vol. 31, no. 2, pp. 291–303. DOI: [10.5194/angeo-31-291-2013](https://doi.org/10.5194/angeo-31-291-2013).
- Mikhailov A.V., Förster M., Leschinskaya T.Y. On the mechanism of the post-midnight winter  $N_mF2$  enhancements: Dependence on solar activity. *Ann. Geophys.* 2000, vol. 18, pp. 1422–1434. DOI: [10.1007/s00585-000-1422-y](https://doi.org/10.1007/s00585-000-1422-y).
- Offermann D., Gusev O., Donner M., Forbes J.M., Hagan M., Mlynczak M.G., Oberheide J., Preusse P., Schmidt H., Russell J.M. III. Relative intensities of middle atmosphere waves. *J. Geophys. Res. Atmos.* 2009, vol. 114, D06110. DOI: [10.1029/2008jd010662](https://doi.org/10.1029/2008jd010662).
- Pedatella N.M., Liu H.-L. Tidal variability in the mesosphere and lower thermosphere due to the El Niño–Southern Oscillation. *Geophys. Res. Lett.* 2012, vol. 39, L19802. DOI: [10.1029/2012gl053383](https://doi.org/10.1029/2012gl053383).
- Pedatella N.M., Liu H.-L. Influence of the El Niño Southern Oscillation on the middle and upper atmosphere. *J. Geophys. Res.: Space Phys.* 2013, vol. 118, pp. 2744–2755. DOI: [10.1002/jgra.50286](https://doi.org/10.1002/jgra.50286).
- Perminov V.I., Semenov A.I., Medvedeva I.V., Zheleznov Y.A. Variability of mesopause temperature from the hydroxyl airglow observations over mid-latitudinal sites, Zvenigorod and Toly, Russia. *Adv. Space Res.* 2014a, vol. 54, pp. 2511–2517. DOI: [10.1016/j.asr.2014.01.027](https://doi.org/10.1016/j.asr.2014.01.027).
- Perminov V.I., Semenov A.I., Medvedeva I.V., Pertsev N.N. Temperature variations in the mesopause region according to the hydroxyl-emission observations at midlatitudes. *Geomagnetism and Aeronomy*. 2014b, vol. 54, pp. 230–239. DOI: [10.1134/s0016793214020157](https://doi.org/10.1134/s0016793214020157).
- Picone J.M., Hedin A.E., Drob D.P., Aikin A.C. NRLMSISE-00 empirical model of the atmosphere: Statistical comparisons and scientific issues. *J. Geophys. Res.* 2002, vol. 107, no. A12, pp. 1468–1483. DOI: [10.1029/2002JA009430](https://doi.org/10.1029/2002JA009430).
- Ratovsky K.G., Medvedev A.V., Tolstikov M.V. Diurnal, seasonal and solar activity pattern of ionospheric variability from Irkutsk Digisonde data. *Adv. Space Res.* 2015, vol. 55, pp. 2041–2047. DOI: [10.1016/j.asr.2014.08.001](https://doi.org/10.1016/j.asr.2014.08.001).
- Ratovsky K.G., Klimenko M.V., Dmitriev A.V., Medvedeva I.V. Relation of extreme ionospheric events with geomagnetic and meteorological activity. *Atmosphere*. 2022, vol. 13, no. 146. DOI: [10.3390/atmos13010146](https://doi.org/10.3390/atmos13010146).
- Rishbeth H., Mendillo M. Patterns of F2-layer variability. *J. Atmos. Solar-Terr. Phys.* 2001, vol. 63, pp. 1661–1680. DOI: [10.1016/s1364-6826\(01\)00036-0](https://doi.org/10.1016/s1364-6826(01)00036-0).
- Ropelewski C.F., Jones P.D. An extension of the Tahiti–Darwin Southern Oscillation Index. *Monthly Weather Review*. 1987, vol. 115, pp. 2161–2165.
- Sassi F., Kinnison D., Boville B.A., Garcia R.R., Roble R. Effect of El Niño–Southern Oscillation on the dynamical, thermal, and chemical structure of the middle atmosphere. *J. Geophys. Res. Atmos.* 2004, vol. 109, D17108. DOI: [10.1029/2003jd004434](https://doi.org/10.1029/2003jd004434).
- Semenov A.I. Variations in the atmospheric temperature response (30–100 km) to solar activity for equatorial and polar latitudes. *Dokl. Earth Sci.* 2008, vol. 423, pp. 1483–1487. DOI: [2008DokES.423.1483S](https://doi.org/2008DokES.423.1483S).
- Semenov A.I., Bakanas V.V., Perminov V.I., Zheleznov Y.A., Khomich Y.V. The near infrared spectrum of the emission of the nighttime upper atmosphere of the Earth. *Geomagnetism and Aeronomy*. 2002, vol. 42, pp. 390–397.
- Shubin V.N., Deminov M.G. Global dynamic model of critical frequency of the ionospheric F2 layer. *Geomagnetism and Aeronomy*. 2019, vol. 59, no. 4, pp. 429–440. DOI: [10.1134/S0016793219040157](https://doi.org/10.1134/S0016793219040157).
- Sun Y.-Y., Liu H., Miyoshi Y., Chang L.C., Liu L. El Niño–Southern Oscillation effect on ionospheric tidal/SPW amplitude in 2007–2015 FORMOSAT-3/COSMIC observations. *Earth Planets Space*. 2019, vol. 71, no. 35. DOI: [10.1186/s40623-019-1009-7](https://doi.org/10.1186/s40623-019-1009-7).
- Zhang S. Ionospheric Climate Change: a report on the ISI team research efforts. Paper presented at the 10<sup>th</sup> Workshop on long-term changes and trends in the atmosphere (Hefei, China, May 14–18, 2018).  
URL: <http://omniweb.gsfc.nasa.gov/form/dx1.html> (accessed August 3, 2022).  
URL: <https://crudata.uea.ac.uk/cru/data/soi/> (accessed October 7, 2022).  
URL: <https://rscf.ru/project/22-17-00146/> (accessed August 3, 2022).  
URL: <http://ckp-rf.ru/ckp/3056/> (accessed August 3, 2022).
- Original Russian version: Zherebtsov G.A., Ratovsky K.G., Medvedeva I.V., published in *Solnechno-zemnaya fizika*. 2024. Vol. 10. No. 4. P. 5–16. DOI: [10.12737/szf-104202401](https://doi.org/10.12737/szf-104202401). © 2024 INFRA-M Academic Publishing House (Nauchno-Izdatelskii Tsentr INFRA-M)

*How to cite this article*

Zherebtsov G.A., Ratovsky K.G., Medvedeva I.V. Long-term variations in peak electron density and temperature of mesopause region: Dependence on solar, geomagnetic, and atmospheric activities, long-term trends. *Solar-Terrestrial Physics*. 2024. Vol. 10. Iss. 4. P. 3–13. DOI: [10.12737/stp-104202401](https://doi.org/10.12737/stp-104202401).